ARTICLE WILEY-VCH

Directing nanostructure formation of gold via the *in situ* under potential deposition of a secondary metal for the detection of nitrite ions

Benchaporn Lertanantawong[‡[a]], Faegheh Hoshyargar[‡[b]] and Anthony P. O'Mullane*[[b]]

Abstract: In this work the underpotential deposition of metals such as copper and lead during the electrochemical deposition of gold is investigated to understand the influence that the incorporation of a second metal has on the morphology of gold nanostructures. The incorporation of Pb or Cu, even at concentrations as low as 0.2 %, significantly influence the morphology of the deposit where the formation of elongated structures from a central gold structure is favoured. These nanostructures are characterised by cyclic voltammetry, X-ray diffraction (XRD), scanning electron microscopy (SEM) and energy-dispersive X-ray spectroscopy (EDX) and tested for their suitability as a sensing layer for the electrochemical detection of nitrite ions in aqueous solution. A limit of detection of 0.3 µM is achieved with a linear range up to 1 mM which is adequate for the determination of nitrite contained within food products.

Introduction

The electrodeposition of nanostructured materials is an area of intense research due to the ability to form highly active surfaces which are not inhibited by surface capping agents.[1-10] The process of electrodeposition or electrochemical restructuring[6, 10-12] of surfaces allows metastable states to be attained and high energy facets to be exposed to solution which aids in both catalytic and electrocatalytic processes. Other advantages include experimental simplicity, control over shape, size and composition and good adherence to underlying supports. There is also significant flexibility in the choice of experimental parameters to achieve the desired material such as time, concentration of metal salt, changing the ionic strength of the electrolyte,[13-14] the applied potential/current profile,[15] the inclusion of surfactants,[16] nanoparticles,[17-18] miscelles,[19] hydrogen bubble templating[5] and use of physical templates such as anodized alumina.[1] The under potential deposition of metals such as copper followed by its galvanic replacement with a more catalytically active metal has also been used as a method to generate active surfaces.[20] In previous work we have demonstrated that the inclusion of lead ions in an electroplating solution has a dramatic effect on the structure of platinum[21] and gold electrodeposits[22] whereby lead was incorporated into the former but not the latter. In addition to the presence of lead ions the generation of halide ions after the reduction of the chloride metal salts, specifically K_2PtCl_6 and $HAuCl_4$ was shown to influence the shape of the final material. A key component to this strategy is the under potential deposition of lead at the growing deposit of either gold or platinum that influences the growth of the metal.

The applicability of nanostructured materials is diverse and encompasses electrocatalysis, photocatalysis and heterogeneous catalysis as well as surface enhanced Raman spectroscopy, nanophotonics, energy storage, additive manufacturing and electrochemical based sensing for a variety of important biological and inorganic analytes.[4, 9-10, 23-31] As an example of the latter, the detection of nitrite has received significant attention.[32-35] Nitrite is an essential component of a healthy diet as it reacts with hemoglobin and produces methemoglobin which enables transporting of oxygen at the cellular level.[36] However excess levels of nitrite in the presence of amines or amides in the stomach convert to nitrosamines which have been reported to be carcinogenic and potentially harmful to humans.[37-38] Therefore, it is important for environmental reasons to monitor nitrite levels as the World Health Organisation (WHO) and the United States Environmental Protection Agency has set limits for the total nitrite content that is allowable in water as well as WHO and EU Scientific Committee for Food recommendations on the amount of nitrite used in foods.[32, 39]

In this work, we investigate the influence of the *in situ* under potential deposition of lead and copper on the electrodeposition of nanostructured gold from gold bromide and chloride salts and investigate the influence that the structure of the deposit has on the electrochemical detection of nitrite.

Results and Discussion

The electrodeposition of gold nanospikes and platinum rich platinum-lead nanostructures from a solution containing $HAuCl_4$ and K_2PtCl_6 with $Pb(CH_3COO)_2$ as the growth directing agent has been demonstrated. To study the effect that other halide metal salts and other metals that are capable of under potential deposition have on the formation of metallic nanostructures we have utilized potassium gold bromide and copper respectively to modify indium tin oxide (ITO) electrodes with gold nanostructures. Figures 1a and b depict the SEM images of gold

[a] Dr. Benchaporn Lertanantawong
Nanoscience and Nanotechnology Graduate Program, King Mongkut's University of Technology Thonburi (KMUTT), 126 Pracha Uthit Rd., Bangmod, Tungkru, Bangkok 10140, Thailand
[b] Dr. F. Hoshyargar, Assoc. Prof. A. P. O'Mullane
School of Chemistry, Physics and Mechanical Engineering
Queensland University of Technology (QUT)
GPO Box 2434, Brisbane, QLD 4001 (Australia)
E-mail: anthony.omullane@qut.edu.au

Supporting information for this article is given via a link at the end of the document.

‡ These authors contributed equally to this work.

nanostructures attained from a solution containing 6.9 mM $KAuBr_4$ in the absence of any growth directing agents. There is a good dispersion of well isolated gold nanoclusters with two clearly distinctive size regimes. The larger nanostructures are quasi spherical consisting of a rough surface made up from agglomerated smaller crystallites. When lead acetate is introduced (Figure 1 c, d), the Pb^{2+} ions influence the growth process and promoted the formation of more evenly sized nanostructures that contain elongated protrusions (Figure 1d). This is consistent with previous work where gold electrodeposited onto gold in the presence of lead acetate resulted in the formation of elongated nanospikes. In that work, the presence of an underlying gold substrate was critical for the formation of a continuous layer of spike like nanomaterials as the interaction of Pb^{2+} ions and liberated chloride ions also occurred also at the substrate as well as the growing gold deposit.

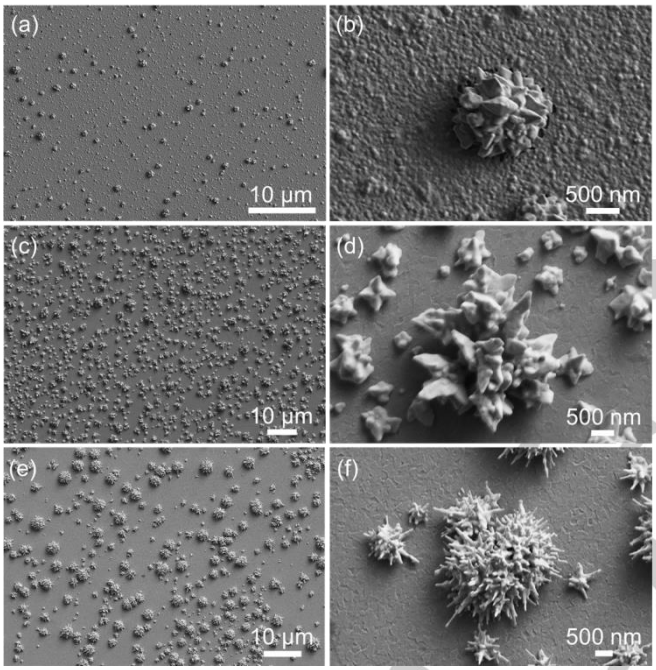

Figure 1. SEM images of samples electrodeposited for 300 s at –0.05 V from 6.9 mM $KAuBr_4$ in the absence (a,b) or presence of 0.5 mM $Pb(CH_3COO)_2$ (c,d) or at 0.15 V in presence of 0.5 mM $CuSO_4.5H_2O$ (e,f).

Therefore, it is apparent here that the presence of lead ions and liberated bromide ions from cleavage of the Au-Br bond in $AuBr_4^-$ behave in a similar manner to produce hierarchical gold nanostructures. To investigate the composition of these nanostructures EDX was carried out and from the mapping and scan experiments it is evident that a small amount of Pb is incorporated into the nanostructures (Figures S1 and S2). This suggests that the upd of lead is occurring during the growth process as bulk deposition of lead occurs at a significantly lower potential on gold.

To investigate this effect, cyclic voltammograms were recorded at ITO electrodes for gold deposition from $KAuBr_4$ in the absence and presence of Pb^{2+} ions (Figure 2). For the former a cathodic peak is seen at 0.20 V followed by a diffusion limited current until the end of the sweep. On the reverse sweep cathodic current is evident until 0 V followed by a rise in current at the end of the sweep due to electrodissolution of gold. This response is typical for the 3 electron reduction of $AuBr_4^-$ to Au^0.[40] Upon the inclusion of Pb^{2+} ions a minor cathodic process appears at -0.26 V which is not seen in the absence of Pb^{2+} ions in solution. The anodic counterpart shows a peak potential at -0.20 V and this response is typical of an upd process. Further evidence for this being Pb upd at Au was provided by recording a cyclic voltammogram at a previously formed gold nanostructured electrode such as that shown in Figure 3d in a solution without $KAuBr_4$ but containing 0.5 mM $Pb(CH_3COO)_2$ with 6.9 mM sodium acetate to keep the ionic strength similar to the deposition conditions (Figure 2b). The upd of lead can be seen by a minor cathodic process at -0.10 V and a more distinct peak at -0.30 V followed by oxidation peaks at 0.01 and 0.60 V. In the absence of the competing gold deposition process the upd processes can now be clearly seen and is similar with previous studies, although five pairs of peaks for Pb upd on Au single crystals were observed.[41] A large hysteresis is observed between the first cathodic process and its anodic counterpart at the most positive potential and from previous work can be related to Pb adsorption on surface defects.[41] Therefore under the electrodeposition conditions employed of -0.05 V for gold nanostructure formation it is apparent that the upd of lead occurs which influences the morphology of the deposit.

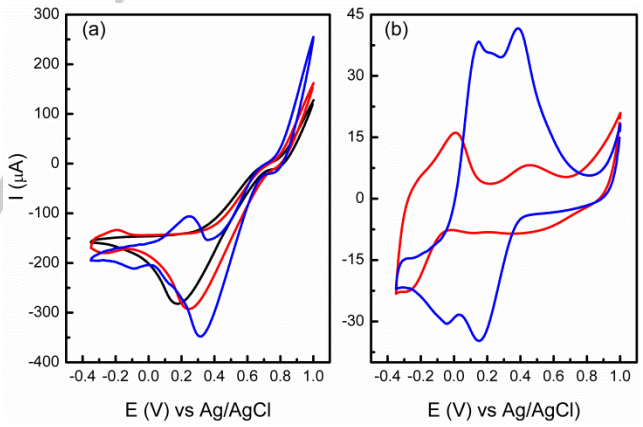

Figure 2. Cyclic voltammograms recorded at an ITO electrode at 50 mV s^{-1} in (a) 6.9 mM $KAuBr_4$ only (black) and containing 0.5 mM $Pb(CH_3COO)_2$ (red) and 0.5 mM $CuSO_4.5H_2O$ (blue); (b) cyclic voltammograms recorded at nanostructured gold (such as Figure 2d) in 6.9 mM CH_3COONa containing 0.5 mM $Pb(CH_3COO)_2$ (red) and 6.9 mM Na_2SO_4 containing 0.5 mM $CuSO_4.5H_2O$ (blue).

To investigate whether the upd of a second metal influences the growth process of gold in a more general way we replaced Pb^{2+} ions with Cu^{2+} as it is well established that Cu upd also occurs on gold.[42-43] Figures 1e and f clearly demonstrate that the presence of Cu^{2+} ions in solution changes the morphology and size of the obtained nanostructures. The upd of

copper is also evident from the cyclic voltammogram shown in Figure 2a where two cathodic peaks with two anodic counterparts are clearly observable which is consistent with Cu adlayer formation on Au ($\sqrt{3}$ x $\sqrt{3}$)*R*30°.[42] As in the case for Pb upd on a nanostructured gold surface the Cu upd processes are more apparent in the absence of the gold salt (Figure 2b) and indicate that the upd of copper will occur during the electrodeposition of gold when carried out at a deposition potential of 0.15 V. Compared to the case when no growth directing agent was used (Figures 1a and b), the addition of Cu^{2+} resulted in the formation of slightly larger nanostructures which resemble sea urchins. The elongated spikes are more defined in this case compared to when Pb^{2+} ions were used (Figure 1d) and range in size from 100 to 500 nm. It should be considered however that the difference in the applied potentials of -0.05 and 0.15 V in the case of Pb^{2+} and Cu^{2+} ions respectively may also slightly affect the surface morphology. These potentials were chosen initially in the study to avoid the upd processes observable in the cyclic voltammograms in Figure 2a. However it is apparent that the upd process will shift to more positive potentials as gold is deposited on the surface of the ITO electrode (Figure 2b). EDX mapping (Figure S3) and the line scan (Figure S4) show that Cu is present in the nanostructures at a level of 0.4% which is larger than the amount of lead incorporation. The presence of a secondary metal shows that it is not only the solution species that play a role in directing the growth of the gold nanostructures. It has been reported that dendritic like structures can be formed when the order associated with crystal symmetry is perturbed by the presence of a foreign species. In this case the presence of copper and/or lead in the growing deposit interferes with the crystal growth of gold and therefore results in the types of structures observed here (Figure 1). When two metals co-crystallise, the lower concentration metal creates pinning centres which induces this disorder and results in the growth of elongated side branches.[44-45]

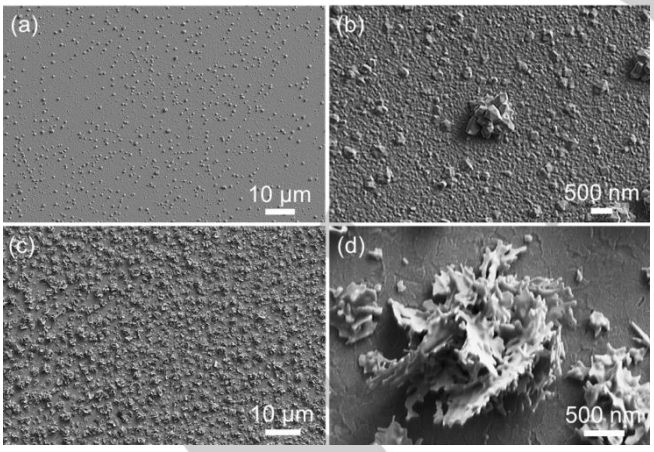

Figure 3. SEM images of samples electrodeposited for 300 s at 0.15 V from 6.9 mM $KAuCl_4$ in the absence (a,b) or presence of 0.5 mM $CuSO_4.5H_2O$ (c,d).

In another set of experiments, gold was electrodeposited from a potassium gold chloride solution in the presence of Cu^{2+} ions following the same procedure to study the effect of the counter ion on the morphology of the electrodeposited Au nanostructures. The morphology of Au nanostructures electrodeposited in the absence of Cu^{2+} ions (Figures 3a and b) are similar to those obtained when potassium gold bromide was used, although the size distribution is narrower. However, in the case of Cu^{2+} ions, very large intertwined plate-like branches arose, which are much larger in diameter compared to the nanostructures obtained when Pb^{2+} or Cu^{2+} ions were used when depositing from an $AuBr_4^-$ solution. EDX analysis revealed 0.2% Cu which was evenly distributed through the material (Figures S5 and S6). The upd of copper was confirmed by cyclic voltammetry experiments (Figure S7) which show a similar profile to that seen for the case of Cu^{2+} ions in the presence of $KAuBr_4$. Therefore it appears that the interplay between the Cu^{2+} ions and the liberated chloride anions also play a contributory role in the growth of the deposit. This may be related to the solubility of copper chloride ($CuCl_2$ and CuCl) and copper bromide ($CuBr_2$ and CuBr) formed at the interface of the growing deposit whereby the chlorides are more soluble than the bromides and therefore in principle would not be as restrictive to the formation of the growing gold electrodeposit.

XRD experiments confirmed that in all cases the electrodeposited gold nanostructures formed in the absence or presence of the Cu^{2+} and Pb^{2+} growth directing agents are polycrystalline with a face centered cubic crystal structure (Figure 4). As evident from the relative intensities, the (111) plane is the dominant growth direction for all of the electrodeposited materials, which is slightly more enhanced when Cu^{2+} and Pb^{2+} ions are used to create the Au nanostructures. This is reflected in the SEM images which show elongated structures and is consistent with growth in the (111) direction.[22]

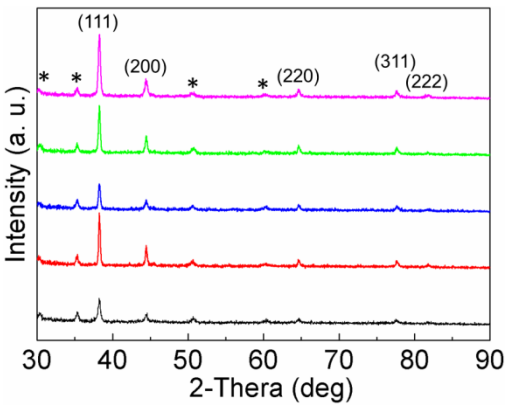

Figure 4. XRD patterns of nanostructured gold samples electrodeposited from $KAuBr_4$ solution in the absence (black) or presence of $Pb(CH_3COO)_2$ (red) or $CuSO_4.5H_2O$ (blue) or from $KAuCl_4$ solution in the absence (green) or presence (pink) of $CuSO_4.5H_2O$. The asterisks indicate reflections from the underlying ITO glass substrate.

The electrochemical behaviour of gold nanostructures electrodeposited from the different gold salts and using Pb^{2+} or Cu^{2+} ions in solution was investigated by undertaking cyclic voltammetry in an acidic electrolyte (Figure 5). In all cases the expected electrochemical profile is seen[46-47] which shows an extended double layer region from 0.0 to 1.0 V followed by monolayer oxide formation on the forward sweep represented as a broad process containing some finer features which is reduced in a sharp cathodic process on the reverse sweep centred at 0.85 V. This sharp cathodic peak occurs at the same potential for all surfaces and is consistent with the low incorporation of the second metal, i.e. Pb or Cu into the deposit. Previous work has shown that higher contents of a second metal, in particular when alloy formation occurs between two metals results in a significant shift in the potential of the oxide reduction peak by up to tens of millivolts,[48-49] which is not seen here. For the case of gold electrodeposited from $AuBr_4^-$ (Figure 5a) there is a clear emergence of a process at ca. 1.05 V when Cu^{2+} and Pb^{2+} ions are used in the synthesis which is indicative of premonolayer oxide formation at nanostructured gold.[3, 46, 50-51] The prominent peak at ca. 1.40 V is indicative of exposed (111) facets[52] which is consistent with the XRD data (Figure 4). These voltammetric features are also apparent when $KAuCl_4$ in the presence of Cu^{2+} ions are used to deposit the nanostructures (Figure 5b). This figure also shows that the surface area of the deposit increases with electrodeposition time as it can be seen that the magnitude of the response for 300 s deposition time exceeds that for 150 s and is consistent with electrodeposition processes. Interestingly, there is a minor peak at ca. 0.30 V in each case where Cu^{2+} ions were used in the electroplating solution. This process most likely originates from the stripping of copper from the deposit which is present at a level of 0.2 to 0.4 % as determined by EDX analysis.

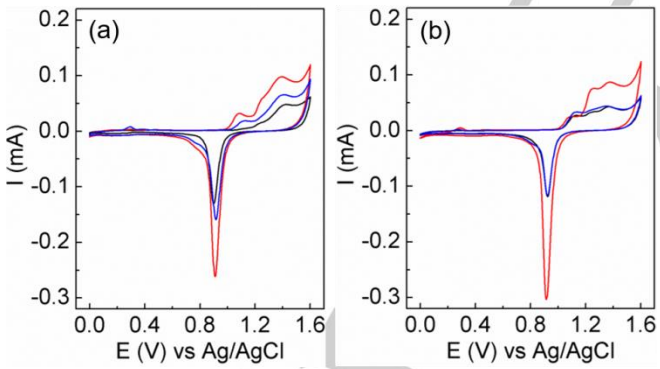

Figure 5. Cyclic voltammograms recorded at an Au nanostructured electrode electrodeposited for 300 s (a) at –0.05 V from 6.9 mM $KAuBr_4$ in the absence (black) or presence of 0.5 mM $Pb(CH_3COO)_2$ (red) or at 0.15 V in presence of 0.5 mM $CuSO_4.5H_2O$ (blue) (b) at 0.15 V from 6.9 mM $KAuCl_4$ in the absence (black) or presence of 0.5 mM $CuSO_4.5H_2O$ for 150 s (blue) or for 300 s (red).

These nanostructures were further investigated for their electrocatalytic properties where the oxidation of nitrite ions in aqueous solution was chosen due to the importance of nitrite ion detection for the food industry. Differential pulse voltammetry was used to maximise sensitivity as well as determine the most active surface for nitrite ion oxidation (Figure 6). A clear peak can be observed at ca. 0.76 V for all electrodes which is consistent with previous reports on the direct electrochemical detection of nitrite ions.[32] The highest current response was obtained with the Au nanostructured electrode obtained from using $KAuBr_4$ bromide with Pb^{2+} ions (Figure 6a, red line). This increased performance is attributed to the higher surface are of this material compared to the other nanostructures (Figure 5a). When Cu^{2+} ions were used to direct growth in the case of electrodeposition from $KAuCl_4$ a similar performance was achieved (Figure 6b, red line) which again is solely due to increased surface area (Figure 5b). However for further analysis of nitrite detection the former sample was investigated in more detail.

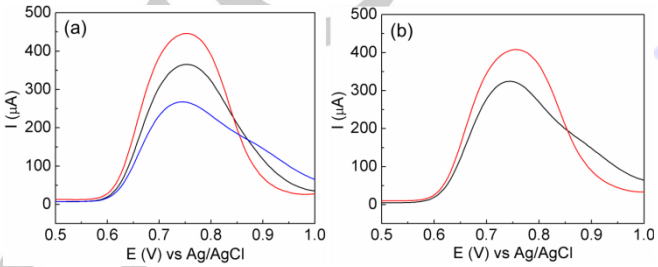

Figure 6. Differential pulse voltammograms recorded in 7 mM $NaNO_2$ at a Au nanostructured electrode electrodeposited for 300 s at a swipe rate of 50 mV s^{-1} (a) at –0.05 V from 6.9 mM $KAuBr_4$ in the absence (black) or presence of 0.5 mM $Pb(CH_3COO)_2$ (red) or at 0.15 V in presence of 0.5 mM $CuSO_4.5H_2O$ (blue) and (b) at 0.15 V from 6.9 mM $KAuCl_4$ in the absence (black) or presence of 0.5 mM $CuSO_4.5H_2O$ (red).

Significantly, the Au nanostructured electrocatalyst demonstrated a linear response over a wide range of nitrite concentration up to 1 mM as seen in Figure 7 which shows a plot of peak height or peak area (Figure 7b) versus concentration. However above this value the linear relationship no longer holds and the response begins to saturate (Figure 7 c and d). However this is not too concerning as the levels of nitrite that need to be detected in drinking water or in foodstuffs is quite low as set by the WHO which is in the less than 3 ppm in drinking water and 30 ppm in processed meat where it is used to give it its red colour.[32]

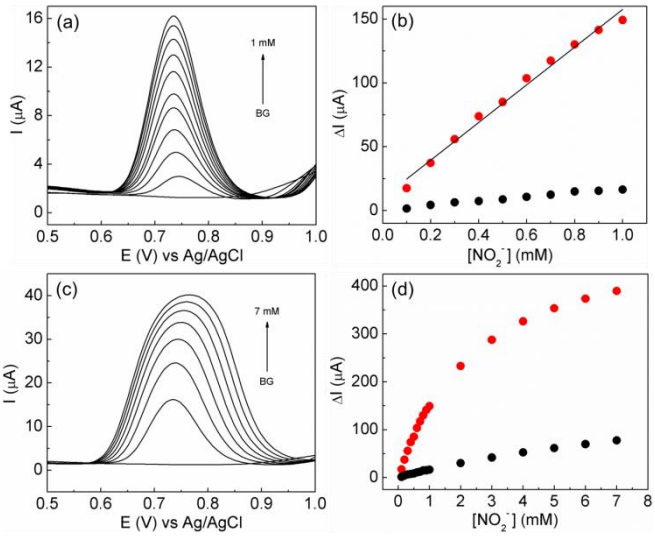

Figure 7. Differential pulse voltammograms (a,c) detailing the determination of nitrite (BG: blank response from Na_2SO_4 buffer) and calibration curve of the response current height (black) or area (red) of the Au modified electrode electrodeposited from $KAuBr_4$ solution in presence of 0.5 mM $Pb(CH_3COO)_2$ to nitrite with different concentrations in the range of 0.1 – 1 mM (a,b) and 1 – 7 mM (c,d).

To probe the sensitivity of the gold nanostructured surface, the detection of nitrite at the micromolar level was undertaken and is shown in Figure 8. There is a good linear relationship from 0 to 5 μM nitrite (regression data $\Delta I/\mu A = 0.9559\ [NO_2^-]/\mu M + 0.6028$, $R^2 = 0.9969$) (Figure 8b) and the limit of detection is 0.3 μM. For a real sample, fresh spinach was chosen as a source of nitrite ions. Figure 8c shows the peak determined for nitrite ion oxidation which equates to 6 ppm nitrite in the original sample. This is consistent with previous studies where the nitrite levels in a variety of foodstuffs including leafy vegetables from different regions in Italy was analysed. Typical ranges for fresh spinach were determined to be 9.5 to 28.5 ppm with this Italian sample (ion chromotagraphy method) whereas a Danish study (spectrophotometric method where nitrite is reacted with sulphanilamide and N-(1-naphthyl)ethylene-diamine to give a coloured solution), and showed levels to be 11 ± 30 ppm.[39]

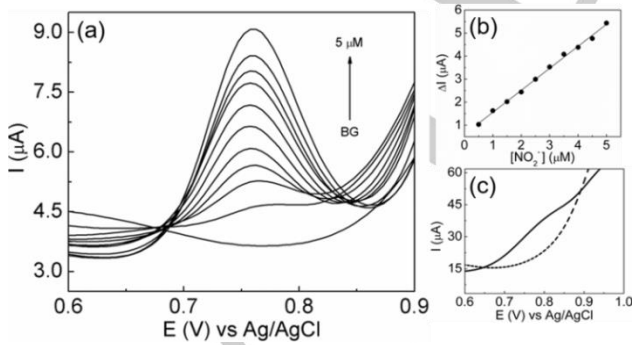

Figure 8. (a) Differential pulse voltammograms detailing the determination of nitrite in the range of 0.5 – 5 μM (BG: blank response from Na_2SO_4 buffer) and (b) calibration curve of the response current of the Au modified electrode electrodeposited from $KAuBr_4$ solution in presence of 0.5 mM $Pb(CH_3COO)_2$ to nitrite with different concentrations in the range of 0.5 – 5 μM, (c) Differential pulse voltammograms recorded in 0.1 M Na_2SO_4 in the absence (dotted) or presence (full line) of 100 μL spinach extract.

Conclusions

It has been demonstrated that the *in situ* upd of Cu or Pb while gold is being electrodeposited on an ITO electrode significantly influences the morphology of the final deposit. The incorporation of a second metal, either Cu or Pb creates pinning centres which disturbs the crystal growth of gold and favours the formation of elongated structures from a central gold deposit where the phenomenon is more pronounced in the case of copper. Cyclic voltammetry studies confirm the XRD analysis that (111) oriented nanostructures are obtained with higher surface area compared to gold structures formed in the absence of the metal upd process. The speciation of the gold salt also played a role and contributed to different morphologies for electrodeposited nanostructures from gold bromide or gold chloride salts. Finally, gold nanostructures were shown to be suitable for the direct detection of nitrite ions in solution with a limit of detection of 0.3 μM and a liner range of up to 1 mM. This was found suitable for the detection of nitrite in leafy vegetables such as spinach where a value of 6 ppm was found. The advantage of the electrochemical approach is that the method is rapid and can be used directly with the solution from the digested sample.

Experimental Section

Materials and chemicals

Potassium tetrabromoaurate(III) hydrate ($KAuBr_4 \cdot xH_2O$, 99.9%), potassium gold(III) chloride ($KAuCl_4$, 99.995%), lead(II) acetate trihydrate ($Pb(CH_3COO)_2 \cdot 3H_2O$, 99.999%), copper(II) sulfate pentahydrate ($CuSO_4 \cdot 3H_2O$, 98%), sodium sulfate (Na_2SO_4, 99%) and sodium nitrite ($NaNO_2$, 97%) were purchased from Sigma-Aldrich. All aqueous solutions were prepared using deionised water (resistivity of 18.2 MΩ.cm at 25°C) purified by use of a Milli-Q reagent deionizer (Millipore). Tin doped indium oxide (ITO) coated glasses (Corning® alkaline earth boro-aluminosilicate glass, 25×25×1.1 mm^3, indium tin oxide coated one surface, R_s = 5 – 15 Ω) were purchased from Delta Technologies, Ltd.

Electrochemical measurements

Cyclic voltammetry experiments were carried out at (25 ± 2)°C using a Metrohm (Autolab PGSTAT128N) electrochemical analyser in an electrochemical cell that allowed reproducible positioning of the working, reference, and counter electrodes and a nitrogen inlet tube. An 8×25×1.1 mm^3 ITO coated glass was used as the working electrode, with the geometric area of the latter defined by the addition of a scotch tape with an exposed circular region of 4.5 mm in diameter. Prior to using ITO coated glass as the working electrode, each sample was sonicated in acetone and then in methanol for 5 min followed by drying in a stream of nitrogen gas prior to use. The reference electrode was Ag/AgCl (aqueous 3 M KCl). For electrodeposition experiments and cyclic voltammetric studies an inert graphite rod (6 mm diameter, Johnson Matthey Ultra 'F' purity grade) was used as the counter electrode. All electrochemical experiments were conducted in 0.1 M Na_2SO_4 and commenced after degassing the electrolyte solutions with nitrogen for at least 10 min prior

to any measurement. Differential pulse voltammetry (DPV) at a sweep rate of 50 mV s^{-1} was also carried out with the Autolab PGSTAT128N potentiostat.

For the spinach sample, fresh spinach was purchased from a local supermarket and used on the same day. 10 g of spinach was reduced and boiled in 5 ml of Milli-Q water for 30 min. 0.1 ml of the solution was injected into 10 ml of Na_2SO_4 electrolyte and DPV carried out to determine the concentration of nitrite.

Material Characterization

Material characterization was performed by using field-emission scanning electron microscopy (FESEM, Zeiss Sigma VP field emission scanning electron microscope equipped with an Oxford XMax 50 Silicon Drift energy-dispersive X-ray detector at 20 kV under high vacuum), and X-ray diffraction BRUKER AXS: D8Discover operating at 40 kV and 40 mA by using CuKα radiation with Goebel Mirror (for parallel beam). Prior to SEM imaging, samples were thoroughly rinsed with Milli-Q water and dried under a flow of nitrogen.

Acknowledgements

B.L. is thankful to Thailand's Office of Higher Education Commission for the National Research University Project (Grant number:59000331) and International Strategic Output & Outcome, KMUTT for research travel support. A.O.M gratefully acknowledges support from the Australian Research Council (Future Fellowship FT110100760). The SEM data reported in this paper were obtained at the Central Analytical Research Facility (CARF), operated by the Institute for Future Environments (QUT). Access to CARF is supported by generous funding from the Science and Engineering Faculty (QUT).

Keywords: Gold nanostructures • under potential deposition • Nitrite detection • metal seed • crystal growth

[1] A. D. Davydov, V. M. Volgin, *Russ. J. Electrochem.*, **2016**, *52*, 806-831.
[2] A. P. O'Mullane, *Nanoscale*, **2014**, *6*, 4012-4026.
[3] B. J. Plowman, A. P. O'Mullane, S. K. Bhargava, *Faraday Discuss.*, **2011**, *152*, 43-62.
[4] B. J. Plowman, S. K. Bhargava, A. P. O'Mullane, *Analyst*, **2011**, *136*, 5107-5119.
[5] B. J. Plowman, L. A. Jones, S. K. Bhargava, *Chem. Commun.*, **2015**, *51*, 4331-4346.
[6] S. Cherevko, N. Kulyk, C.-H. Chung, *Nanoscale*, **2012**, *4*, 568-575.
[7] W. Ye, J. Yan, Q. Ye, F. Zhou, *J. Phys. Chem. C*, **2010**, *114*, 15617-15624.
[8] I.-W. Sun, J.-K. Chang, in *Springer Handbook of Electrochemical Energy*, eds. C. Breitkopf and K. Swider-Lyons, Springer Berlin Heidelberg, Berlin, Heidelberg, 2017, pp. 835-895.
[9] O. A. Petrii, *Russ. Chem. Rev.*, **2015**, *84*, 159.
[10] J. Duay, E. Gillette, J. Hu, S. B. Lee, *Phys. Chem. Chem. Phys.*, **2013**, *15*, 7976-7993.
[11] N. Tian, Z.-Y. Zhou, S.-G. Sun, Y. Ding, Z. L. Wang, *Science*, **2007**, *316*, 732-735.
[12] A. Balkis, A. P. O'Mullane, *Aus. J. Chem.*, **2015**, *68*, 1213-1220.
[13] C. Liu, Y. Long, S. Magdassi, D. Mandler, *Nanoscale*, **2017**, *9*, 485-490.
[14] A. K. Pearson, P. Kao, A. P. O'Mullane, A. I. Bhatt, *Phys. Chem. Chem. Phys.*, **2017**, *19*, 14745-14760.
[15] R. Sivasubramanian, M. V. Sangaranarayanan, *CrystEngComm*, **2013**, *15*, 2052-2056.
[16] T.-H. Lin, C.-W. Lin, H.-H. Liu, J.-T. Sheu, W.-H. Hung, *Chem. Commun.*, **2011**, *47*, 2044-2046.
[17] A. Pearson, A. P. O'Mullane, *Chem. Commun.*, **2015**, *51*, 5410-5413.
[18] B. Lertanantawong, W. Surareungchai, A. P. O'Mullane, *J. Electroanal. Chem.*, **2016**, *779*, 99-105.
[19] S. Saha, S. Sultana, M. M. Islam, M. M. Rahman, M. Y. A. Mollah, M. A. B. H. Susan, *Ionics*, **2014**, *20*, 1175-1181.
[20] A. Papaderakis, I. Mintsouli, J. Georgieva, S. Sotiropoulos, *Catalysts*, **2017**, *7*, 80.
[21] B. Plowman, M. Abdelhamid, S. Ippolito, V. Bansal, S. Bhargava, A. O'Mullane, *J. Solid State Electrochem.*, **2014**, *18*, 3345-3357.
[22] B. Plowman, S. J. Ippolito, V. Bansal, Y. M. Sabri, A. P. O'Mullane, S. K. Bhargava, *Chem. Commun.*, **2009**, 5039-5041.
[23] R. M. Penner, *J. Phys. Chem. C*, **2014**, *118*, 17179-17192.
[24] Q. Luo, M. Peng, X. Sun, Y. Luo, A. M. Asiri, *Int. J. Hydrogen Energy*, **2016**, *41*, 8785-8792.
[25] S. Murugesan, A. Akkineni, B. P. Chou, M. S. Glaz, D. A. Vanden Bout, K. J. Stevenson, *ACS Nano*, **2013**, *7*, 8199-8205.
[26] J. Liu, L. Cao, Y. Xia, W. Huang, Z. Li, *Int. J. Electrochem. Sci.*, **2013**, *8*, 9435-9441.
[27] M. A. Sayeed, T. Herd, A. P. O'Mullane, *J. Mater. Chem. A*, **2016**, *4*, 991-999.
[28] T. M. Braun, D. T. Schwartz, *The Electrochemical Society Interface*, **2016**, *25*, 69-73.
[29] I. Najdovski, P. R. Selvakannan, A. P. O'Mullane, *RSC Adv.*, **2014**, *4*, 7207-7215.
[30] J. Elias, M. Gizowska, P. Brodard, R. Widmer, Y. deHazan, T. Graule, J. Michler, L. Philippe, *Nanotechnology*, **2012**, *23*, 255705.
[31] S. Paul, *Nanomaterials and Energy*, **2015**, *4*, 80-89.
[32] Y. Zhang, F. Cheng, M. Zhang, P. Liu, M. Chen, Z. Cai, *J. Electroanal. Chem.*, **2016**, *773*, 1-6.
[33] Y. Li, C. Sella, F. Lemaître, M. Guille Collignon, L. Thouin, C. Amatore, *Electroanalysis*, **2013**, *25*, 895-902.
[34] Y.-X. Chen, S.-P. Chen, Q.-S. Chen, Z.-Y. Zhou, S.-G. Sun, *Electrochim. Acta*, **2008**, *53*, 6938-6943.
[35] J. Davis, M. J. Moorcroft, S. J. Wilkins, R. G. Compton, M. F. Cardosi, *Analyst*, **2000**, *125*, 737-742.
[36] M. Rezaei, A. Fani, A. L. Moini, P. Mirzajani, A. A. Malekirad, M. Rafiei, *International Scholarly Research Notices*, **2014**, *2014*, 5.
[37] M. Iammarino, A. Di Taranto, M. Cristino, *J. Sci. Food Agriculture*, **2014**, *94*, 773-778.
[38] M. S. Shailaja, R. Rajamanickam, S. Wahidulla, *Environmental Pollution*, **2006**, *143*, 174-177.
[39] A. Petersen, S. Stoltze, *Food Additives & Contaminants*, **1999**, *16*, 291-299.
[40] A. Pearson, A. P. O'Mullane, V. Bansal, S. K. Bhargava, *Chem. Commun.*, **2010**, *46*, 731-733.
[41] A. J. Motheo, E. R. Gonzalez, G. Tremilliosi-Filho, A. Rakotondrainibe, J.-M. Léger, B. Beden, C. Lamy, *J. Braz. Chem. Soc.*, **1998**, *9*, 31-38.
[42] E. Herrero, L. J. Buller, H. D. Abruña, *Chem Rev.*, **2001**, *101*, 1897-1930.
[43] D. Krznarić, T. Goričnik, *Langmuir*, **2001**, *17*, 4347-4351.
[44] J. Wang, R. M. Asmussen, B. Adams, D. F. Thomas, A. Chen, *Chem. Mater.*, **2009**, *21*, 1716-1724.
[45] A. Balkis, A. P. O'Mullane, *Mater. Chem. Phys.*, **2014**, *143*, 747-753.
[46] B. Lertanantawong, A. P. O'Mullane, W. Surareungchai, M. Somasundrum, L. D. Burke, A. M. Bond, *Langmuir*, **2008**, *24*, 2856-2868.
[47] L. D. Burke, J. M. Moran, P. F. Nugent, *J. Solid State Electrochem.* , **2003**, *7*, 529-538.
[48] J. B. Xu, T. S. Zhao, S. Y. Shen, Y. S. Li, *Int. J. Hydrogen Energy*, **2010**, *35*, 6490-6500.
[49] S.-M. Hwang, J. E. Bonevich, J. J. Kim, T. P. Moffat, *J. Electrochem. Soc.*, **2011**, *158*, B1019-B1028.
[50] L. D. Burke, L. M. Hurley, V. E. Lodge, M. B. Mooney, *J. Solid State Electrochem.*, **2001**, *5*, 250-260.
[51] L. D. Burke, P. F. Nugent, *Gold Bulletin*, **1997**, *30*, 43-53.
[52] M. A. Schneeweiss, D. M. Kolb, D. Liu, D. Mandler, *Can. J. Chem.*, **1997**, *75*, 1703-1709.

ARTICLE

The underpotential deposition of copper and lead during the course of gold electrodeposition results in the formation of flower like nanomaterials that are suitable as a sensing layer for the detection of nitrite ions.

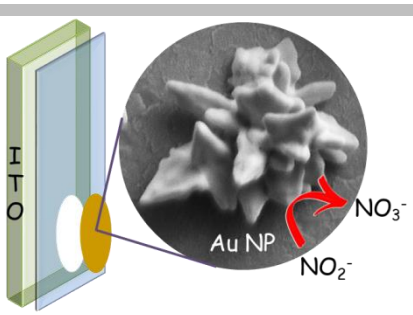

*Benchaporn Lertanantawong, Faegheh Hoshyargar, Anthony P. O'Mullane**

Page No. – Page No.
Directing nanostructure formation of gold via the *in situ* under potential deposition of a secondary metal for the detection of nitrite ions